2008 IEEE International Conference on
Robotics and Automation
Pasadena, CA, USA, May 19-23, 2008

Elasto-Geometrical Modelling of Closed-Loop Industrial Robots Used For Machining Applications

S. Marie, P. Maurine

***Abstract*— This paper presents the elasto-geometrical modelling of an industrial robot manipulator whose structure includes a closed-loop mechanism. This modelling is done for sensitivity studies and calibration purposes since the robot is involved in machining operations that require a high level of quasi static positioning accuracy. The kinematics of the machine is described first then the systematic approach that is proposed to calculate the elastic modelling of its architecture is presented. Simulations and experiments are presented next in order to evaluate the limitations and benefits of the proposed modelling approach.**

I. Introduction

Nowadays, some industrial robots manipulators are used for machining applications. These applications usually involve some large, complex parts to be machined on a 4- or 5- axis machining centers. As explained in [1], these parts are usually made of soft material such as plastics, fibreglass, carbon-fiber composites and materials used for prototyping. When it comes to machining metals, most parts require precision machining. As a result, considering the today's robots positioning accuracy, there are some applications in which this accuracy is acceptable such as rough machining parts to prepare them for finish cutting on CNC machine tools. However for the others, both robot torque and positioning accuracy have to be significantly increased. The increased torque that robots need for metal machining can be obtained with more powerful spindles. However, for hard materials as metal, robots have then to be strong and mechanically stiff and rigid to withstand the machining forces. Moreover in terms of modelling the elasto-geometrical behaviour of their mechanical structure has to be accurately known in order to compensate, with the control, the effects of the remaining elastic deformations of the robot links and joints onto the positioning accuracy [2-6]. This is in this context that the presented works take place. The purpose of this paper is to present an original approach to derive the elasto geometrical model of an industrial robot with a closed-loop chain used to increase the stiffness of its structure.

The paper is organised as follows. The kinematics and geometrical error model of the KUKA IR663 closed-loop robot on which the study focuses are described first.

S. Marie is with LGCGM EA-3913 / INSA de Rennes,
20, Av. des Buttes de Coësmes, CS 14315 F-35043 Rennes Cedex, France
(e-mail : stephane.marie@ens.insa-rennes.fr)
P. Maurine is with LGCGM EA-3913 / INSA de Rennes
20, Av. des Buttes de Coësmes, CS 14315 F-35043 Rennes Cedex, France
(e-mail : patrick.maurine@insa-rennes.fr)

Then the systematic approach that is proposed to calculate the elastic modelling of its architecture is presented. Simulations and experimental tests are presented next in order to evaluate the limitations and benefits of the proposed modelling approach.

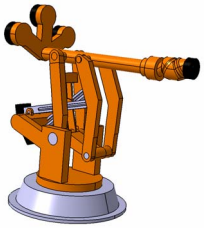

Fig. 1. KUKA IR663.

II. KUKA IR663 Kinematics

The KUKA IR663 that has been used is shown on Fig. 1. This robot architecture has been chosen for the study since:

i) The closed-loop kinematic chain of its structure increases the global stiffness of the robot which fits well with the machining applications that we are interested in.
ii) To our thinking it is one of the most complicated structures of industrial robots that can be modelled.

Its kinematic structure can be described by Fig. 1 and Fig. 2. It has a special wrist made of 4 revolute joints among which two are coupled (biconic wrist). The wrist is carried by an articulated mechanical structure with 6 revolute joints. If n denotes the number of links excluding the one attached to the ground, the global robot structure has thus a number $L = 10$ joints and $n+1 = 10$ links where link 0 is the fixed base and $B = L - n = 1$ closed loop. This loop is a four-bar linkage; two of those links are actuated by a slider-crank type mechanism as illustrated by Fig. 5. The number N of active joints is equal to 6 that corresponds to the number of degrees of freedom of the robot.

In order to derive the geometrical models of the structure that are required to establish the elastic model, the Khalil and Kleinfinger notation [7, 8] is used. The global structure is first described by an equivalent tree structure that is obtained by cutting the closed loop at joint 10 (see Fig. 2). The total number of frames that will be used is equal to $n+1+2B = 12$ (R_0 is the reference frame) since 2 frames have been added while cutting the joint 10 and it is to be noted that the geometric parameters used to locate the frame 11 relatively to the frame 9 are fixed.

The whole structure can be described by Table I. The joint j connects link j to the link $a(j)$ where $a(j)$ denotes the link antecedent to the link j and the topology of the structure is

defined by $a(j)$ for $j = 1, ..., 11$. The situation of the end-effector E mounted on the link 7 corresponds to the line $j = E$ in the table. The parameter μ_j equals 1 if the joint j is active and 0 if it is passive. In order to calculate the mathematical relationships required to locate all the links, a frame R_i attached to each link i is defined as follows:

- $\mathbf{z}_i$ is along the axis of the joint i;
- $\mathbf{x}_i$ is taken along the common normal between $\mathbf{z}_i$ and one of the succeeding joint axis that are fixed on link i.

If $\mathcal{R}$ and $\mathcal{T}$ denote respectively the homogeneous matrices of rotation and translation, the homogeneous transformation matrix ${}^{i}\mathbf{T}_j$ that describes the location of the frame R_j relative to frame R_i such as $i = a(j)$ is calculated according to:

$$- {}^{i}\mathbf{T}_j = \mathcal{R}(\mathbf{x},\alpha_j)\mathcal{T}(\mathbf{x},d_j)\mathcal{R}(\mathbf{z},\theta_j)\mathcal{T}(\mathbf{z},r_j) \quad (1)$$

if $\mathbf{x}_i$ is taken along the common normal between $\mathbf{z}_i$ and $\mathbf{z}_j$.

$$- {}^{i}\mathbf{T}_j = \mathcal{R}(\mathbf{z},\gamma_j)\mathcal{T}(\mathbf{z},b_j)\mathcal{R}(\mathbf{x},\alpha_j)\mathcal{T}(\mathbf{x},d_j)\mathcal{R}(\mathbf{z},\theta_j)\mathcal{T}(\mathbf{z},r_j) \quad (2)$$

if $\mathbf{x}_i$ is not taken along the common normal between $\mathbf{z}_i$ and $\mathbf{z}_j$. In that case, the description of the situation of R_j relative to the frame R_i requires six geometrical parameters α_j, d_j, θ_j, r_j, γ_j and b_j.

The definition of these geometrical parameters is available in [8]. The numerical values for the Kuka IR663 are given in Table II.

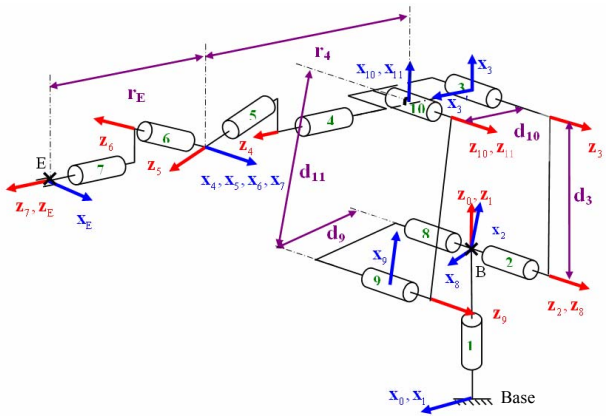

Fig. 2. Linkage, frames and notations.

TABLE I
GEOMETRICAL PARAMETERS OF THE KUKA IR663.

j	a(j)	μ_j	γ_j	b_j	α_j	d_j	θ_j	r_j
1	0	1	0	0	0	0	θ_1	0
2	1	1	0	0	$-\pi/2$	0	$\theta_2 - \pi/2$	0
3	2	0	0	0	0	d_3	θ_3	0
4	3	1	0	0	$-\pi/2$	0	$\theta_4 - \pi/2$	$r_4 + d_{10}$
5	4	1	0	0	$\pi/6$	0	θ_5	0
6	5	0	0	0	$-\pi/3$	0	$\theta_6 = -\theta_5$	0
7	6	1	0	0	$\pi/6$	0	θ_7	0
8	1	1	0	0	$-\pi/2$	0	θ_8	0
9	8	0	0	0	0	d_9	θ_9	0
10	3	0	$\pi/2$	0	0	d_{10}	$\theta_{10} - \pi/2$	0
11	9	0	0	0	0	d_{11}	$\theta_{11} = 0$	0
E	7	0	0	0	0	0	0	r_E

TABLE II
NUMERICAL VALUES OF GEOMETRICAL PARAMETERS.

Parameter	r_1	d_3	r_4	d_9	d_{10}	d_{11}	r_E
Numerical Value (mm)	885	1047	1760	473	400	1212	244

III. GEOMETRICAL MODELS

In this part, the approach used to derive the geometrical models of the robot is presented. In spite of many works have been already achieved on the calibration of closed-loops robots [2, 9, 10], these explanations are, to our thinking, useful to well understand the kinematics of the robot structure before introducing the systematic method that we propose to derive the elastic model of its structure.

A. Forward and Inverse Geometrical Models

In order to derive the Forward and Inverse Geometrical Models of the structure (FGM, IGM), one has to establish the mathematical relation connecting the situation of the frame R_E attached to the end-effector E (spindle) to the situation of the actuated robot joints. For that purpose, one open kinematic chain has been selected after cutting the joint 10 as represented in bold on Fig. 3.

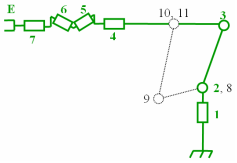

Fig. 3. Kinematic chain for the FGM calculation.

By writing the homogeneous matrices describing the relative situation of the frames of that chain and by multiplying them, the relation from which the FGM and IGM are deduced is obtained:

$${}^{0}\mathbf{T}_E = {}^{0}\mathbf{T}_1(\theta_1)\,{}^{1}\mathbf{T}_2(\theta_2)\,{}^{2}\mathbf{T}_3(\theta_3)\,{}^{3}\mathbf{T}_4(\theta_4)\,{}^{4}\mathbf{T}_5(\theta_5)\,{}^{5}\mathbf{T}_6(\theta_6)\,{}^{6}\mathbf{T}_7(\theta_7)\,{}^{7}\mathbf{T}_E \quad .(3)$$

The matrix ${}^{0}\mathbf{T}_E$ gives the situation of E within R_0. However, as one can see, the joints 3 and 6 are passive and relations linking their values to the actuated joints values of the robot have to be calculated (see Fig. 4).

For that purpose, the trivial relation expressing the fact that the rotation angle of the wrist joints 5 and 6 are of opposite sign is written:

$$\theta_6 = -\theta_5 \,. \quad (4)$$

Then the relation F is derived in order to link the value of θ_3 to the actuated joint values θ_2, θ_8 and the geometrical parameters of the four-bar linkage d_3, d_9, d_{10} and d_{11}:

$$\theta_3 = F(\theta_2, \theta_8, d_3, d_9, d_{10}, d_{11}) \,. \quad (5)$$

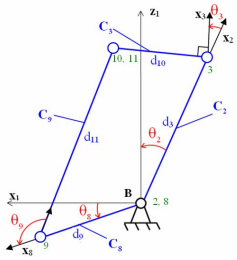

Fig. 4. Description of the four-bar linkage.

For the calculation of F, we made the assumption that the four bar linkage is a plane mechanism. In other words, the axes of the joints 2, 3, 8, 9 and 10 are perfectly parallel. As well, in a first approach, the joints 2 and 8 are seen as revolute ones. Then by using the closure equation of the linkage ${}^{11}\mathbf{T}_9\,{}^{9}\mathbf{T}_8\,{}^{8}\mathbf{T}_1\,{}^{1}\mathbf{T}_2\,{}^{2}\mathbf{T}_3\,{}^{3}\mathbf{T}_{10} = \mathbf{I}_4$, the value of θ_3 is calculated as a function of the other loop parameters as follows:

$$\theta_3 = \mathrm{Atan2}\left(\sin(\theta_3), \cos(\theta_3)\right)$$

with: $$\sin(\theta_3) = \frac{B_1 B_3 - B_2\sqrt{B_1^2 + B_2^2 - B_3^2}}{B_1^2 + B_2^2},$$

$$\cos(\theta_3) = \frac{B_2 B_3 - B_1\sqrt{B_1^2 + B_2^2 - B_3^2}}{B_1^2 + B_2^2},$$

$$B_1 = 2Z_2 X,\ B_2 = -2Z_2 Y,\ B_3 = W^2 - X^2 - Y^2 - Z_2^2,$$

and: $$X = d_9\cos(\theta_2 - \theta_8),\ Y = d_3 - d_9\sin(\theta_2 - \theta_8),$$

$$Z_1 = 0,\ Z_2 = -d_{10},\ W = -d_{11}.$$

As the joints 2 and 8 are actuated by ball screws, the relations linking the actuated translational displacements r_2' and r_8' and the parameters of the screws to the joint values θ_2 and θ_8 have been written. These two actuating systems viewed as slider crank type mechanism are described by Fig. 5.

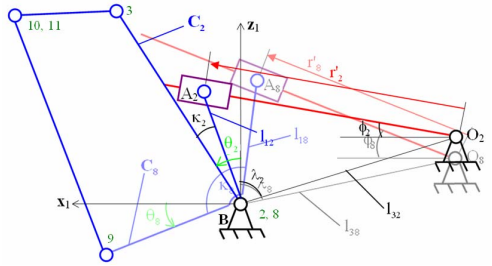

Fig. 5. Ball screws for the actuation of joints 2 and 8.

For θ_2, by writing the closure equation of the mechanism in the plane, the following relations is obtained:

$$\theta_2 = \mathrm{G}\left(r_2', \kappa_2, \lambda_2, l_{12}, l_{32}\right) \qquad (6)$$

with: $$\theta_2 = \kappa_2 - \mathrm{Atan2}\left(\sin(\theta_2), \cos(\theta_2)\right) + \frac{\pi}{2},$$

$$\sin(\theta_2) = \frac{X_2 Z_2 + Y_2\sqrt{X_2^2 + Y_2^2 - Z_2^2}}{X_2^2 + Y_2^2},$$

$$\cos(\theta_2) = \frac{Y_2 Z_2 - X_2\sqrt{X_2^2 + Y_2^2 - Z_2^2}}{X_2^2 + Y_2^2}$$

and: $$X_2 = 2y_B l_{12} \qquad x_B = l_{32}\cos\left(\frac{\pi}{2} - \lambda_2\right)$$

$$Y_2 = 2x_B l_{12}$$

$$Z_2 = r_2' - x_B^2 - y_B^2 - l_{12}^2 \qquad y_B = l_{32}\sin\left(\frac{\pi}{2} - \lambda_2\right)$$

The same approach is applied to the slider crank mechanism that drives the joint 8 in order to calculate the function H linking θ_8 and the ball screw parameters:

$$\theta_8 = \mathrm{H}\left(r_8', \kappa_8, \lambda_8, l_{18}, l_{38}\right). \qquad (7)$$

By using the relations (3), (4), (5), (6) and (7), the situation $\mathbf{X}_E$ of R_E defined by both the position of its origin $\mathbf{P}_E$ and its orientation $\boldsymbol{\Psi}_E$ within R_0 is computed with the FGM through the relation:

$$\mathbf{X}_E = \begin{bmatrix} \mathbf{P}_E \\ \boldsymbol{\Psi}_E \end{bmatrix} = \mathrm{FGM}(\mathbf{q}, \boldsymbol{\xi}). \qquad (8)$$

And for the IGM (obtained with Paul's method), it comes:

$$\mathbf{q} = \mathrm{IGM}(\mathbf{X}_E, \boldsymbol{\xi}), \qquad (9)$$

where:

- $\mathbf{q} = \left[\theta_1, r_2', r_8', \theta_4, \theta_5, \theta_7\right]^T$ stands for the (6x1) vector of actuated joint values.
- $\boldsymbol{\xi}$ is the (37x1) vector of KUKA geometrical parameters (including also the all ball screw parameters) defined by:

$$\boldsymbol{\xi} = [\alpha_1\ d_1\ r_1\ \alpha_2\ d_2\ r_2\ \kappa_2\ \lambda_2\ l_{12}\ l_{32}\ \beta_3\ \alpha_3\ d_3\ r_3\ \alpha_4\ d_4\ r_4\ \alpha_5\ d_5\ r_5\ \alpha_6\ d_6\ r_6\ \alpha_7\ d_7\ r_7\ \beta_E\ \alpha_E\ d_E\ r_E\ \kappa_8\ \lambda_8\ l_{18}\ l_{38}\ d_9\ d_{10}\ d_{11}]^T.$$

B. Error Model for the Geometrical Calibration

For a joint configuration $\mathbf{q}_k$ of the KUKA, the situation $\mathbf{X}_{E,k}$ of E (8) usually differs from the real situation $\mathbf{X}_{E,k}^r$. The resulting positioning error $\Delta\mathbf{X}_{E,k} = \mathbf{X}_{E,k}^r - \mathbf{X}_{E,k}$ can be due to the errors on the geometrical parameters such as the offsets in the actuated joints but also the assembly and manufacturing errors of all robot links. In order to enhance the robot accuracy for machining, the effects of these errors have to be studied and compensated through calibration process [11, 12]. For this purpose, a geometrical error model is derived by calculating for each situation k, the generalized Jacobian matrix $\mathbf{J}_{G,k}$ linking the positioning error $\Delta\mathbf{X}_{E,k}$ to the vector of the geometrical errors $\Delta\boldsymbol{\eta}$ according to the relation:

$$\Delta\mathbf{X}_{E,k} = \mathbf{J}_{G,k}\Delta\boldsymbol{\eta}. \qquad (10)$$

The columns of $\mathbf{J}_{G,k}$ are computed by considering the variations of each geometrical parameter involved in the homogeneous matrices ${}^{i}\mathbf{T}_j$ used to describe the kinematic chain of Fig. 3. As a result $\mathbf{J}_{G,k}$ can be viewed as the concatenation of submatrices as follows:

$$\mathbf{J}_{G,k} = \left[\mathbf{J}_{1,k}\ \ \mathbf{J}_{2,k}\ \ \mathbf{J}_{3,k}\ \ \mathbf{J}_{4,k}\ \ \mathbf{J}_{5,k}\ \ \mathbf{J}_{6,k}\ \ \mathbf{J}_{7,k}\ \ \mathbf{J}_{E,k}\right].$$

$\mathbf{J}_{j,k}$ are the submatrices corresponding to ${}^{i}\mathbf{T}_j$ for j = 1, 2, 3, 4, 5, 6, 7 and E. The calculation of the columns of each submatrix $\mathbf{J}_{j,k}$ is related to the expression of ${}^{i}\mathbf{T}_j$. All these homogeneous transformations are calculated according to the relation (1) excepting the one used to describe the situation of frame R_3 with respect to R_2. For that one the following relation is involved:

$${}^{2}\mathbf{T}_{3,k} = \boldsymbol{\mathcal{R}}(\mathbf{y}, \beta_3)\boldsymbol{\mathcal{R}}(\mathbf{x}, \alpha_3)\boldsymbol{\mathcal{T}}(\mathbf{x}, d_3)\boldsymbol{\mathcal{R}}(\mathbf{z}, \theta_{3,k})\boldsymbol{\mathcal{T}}(\mathbf{z}, r_3).$$

In that case, the parameter β_3 allows considering small orientation errors between the joint axes 2 and 3 which are assumed to be parallel [13]. This will represent the possible orientation errors of the whole four bar linkage with respect to the rest of the open kinematic chain. It comes for the expression of the submatrix $\mathbf{J}_{3,k}$:

$$\mathbf{J}_{3,k} = \begin{bmatrix} \mathbf{J}_{\beta_{3,k}} & \mathbf{J}_{\alpha_{3,k}} & \mathbf{J}_{d_{3,k}} & \mathbf{J}_{\theta_{3,k}} & \mathbf{J}_{r_{3,k}} \end{bmatrix}.$$

For j = 1, 2, 4, 5, 6 and 7, the parameter β_j is not used and $\mathbf{J}_{j,k}$ is defined as follows:

$$\mathbf{J}_{j,k} = \begin{bmatrix} \mathbf{J}_{\alpha_{j,k}} & \mathbf{J}_{d_{j,k}} & \mathbf{J}_{\theta_{j,k}} & \mathbf{J}_{r_{j,k}} \end{bmatrix}.$$

For size considerations of the paper the details of the calculation of the columns $\mathbf{J}_{\beta_{i,k}}$, $\mathbf{J}_{\alpha_{i,k}}$, $\mathbf{J}_{d_{i,k}}$, $\mathbf{J}_{\theta_{i,k}}$ and $\mathbf{J}_{r_{i,k}}$ are not given here but they are available in [8].

At this point, the relations (4), (5), (6), and (7) have to be considered since the geometrical parameters of which they are function of can also be affected by some errors. Since these errors decrease the global accuracy of the robot, they have to be included in the vector $\Delta\boldsymbol{\eta}$ and their related column have to added to the generalized Jacobian matrix $\mathbf{J}_{G,k}$. This has been done by differentiating those relations with respect to the geometrical parameters. The results can be written as follows:

$$d\theta_5 = -d\theta_6, \tag{11}$$

$$d\theta_{3,k} = a_{3,k}\left(d\theta_2 - d\theta_8\right) + b_{3,k}dd_3 + c_{3,k}dd_9 + d_{3,k}dd_{10} + e_{3,k}dd_{11}, \tag{12}$$

$$d\theta_{2,k} = a_{2,k}dr_2' + b_{2,k}d\kappa_2 + c_{2,k}d\lambda_2 + d_{2,k}dl_{12} + e_{2,k}dl_{32}, \tag{13}$$

$$d\theta_{8,k} = a_{8,k}dr_8' + b_{8,k}d\kappa_8 + c_{8,k}d\lambda_8 + d_{8,k}dl_{18} + e_{8,k}dl_{38}. \tag{14}$$

The analytical values of $a_{m,k}$, $b_{m,k}$, $c_{m,k}$, $d_{m,k}$ and $e_{m,k}$ (m = 2, 3, 8) have been obtained using symbolic Matlab® Software and have been merged into the expression of $\mathbf{J}_{G,k}$ of equation (10). The resulting formulation of $\mathbf{J}_{G,k}$ can be written as follows:

$$\mathbf{J}'_{G,k} = \begin{bmatrix} \mathbf{J}'_{1,k} & \mathbf{J}'_{2,k} & \mathbf{J}'_{3,k} & \mathbf{J}'_{4,k} & \mathbf{J}'_{5,k} & \mathbf{J}'_{6,k} \\ \mathbf{J}'_{7,k} & \mathbf{J}'_{E,k} & \mathbf{J}'_{8,k} & \mathbf{J}'_{9,k} & \mathbf{J}'_{10,k} & \mathbf{J}'_{11,k} \end{bmatrix}, \tag{15}$$

where:

$$\mathbf{J}'_{1,k} = \begin{bmatrix} \mathbf{J}_{\alpha_{1,k}} & \mathbf{J}_{d_{1,k}} & \mathbf{J}_{\theta_{1,k}} & \mathbf{J}_{r_{1,k}} \end{bmatrix},$$

$$\mathbf{J}'_{2,k} = \begin{bmatrix} \mathbf{J}_{\alpha_{2,k}} & \mathbf{J}_{d_{2,k}} & \mathbf{J}_{r_{2,k}} & a_{2,k}\left(\mathbf{J}_{\theta_{2,k}} + a_{3,k}\mathbf{J}_{\theta_{3,k}}\right) & b_{2,k}\left(\mathbf{J}_{\theta_{2,k}} + a_{3,k}\mathbf{J}_{\theta_{3,k}}\right) \\ c_{2,k}\left(\mathbf{J}_{\theta_{2,k}} + a_{3,k}\mathbf{J}_{\theta_{3,k}}\right) & d_{2,k}\left(\mathbf{J}_{\theta_{2,k}} + a_{3,k}\mathbf{J}_{\theta_{3,k}}\right) & e_{2,k}\left(\mathbf{J}_{\theta_{2,k}} + a_{3,k}\mathbf{J}_{\theta_{3,k}}\right) \end{bmatrix},$$

$$\mathbf{J}'_{3,k} = \begin{bmatrix} \mathbf{J}_{\beta_{3,k}} & \mathbf{J}_{\alpha_{3,k}} & \left(\mathbf{J}_{d_{3,k}} + b_{3,k}\mathbf{J}_{\theta_{3,k}}\right) & \mathbf{J}_{r_{3,k}} \end{bmatrix},$$

$$\mathbf{J}'_{4,k} = \begin{bmatrix} \mathbf{J}_{\alpha_{4,k}} & \mathbf{J}_{d_{4,k}} & \mathbf{J}_{\theta_{4,k}} & \mathbf{J}_{r_{4,k}} \end{bmatrix},$$

$$\mathbf{J}'_{5,k} = \begin{bmatrix} \mathbf{J}_{\alpha_{5,k}} & \mathbf{J}_{d_{5,k}} & \left(\mathbf{J}_{\theta_{5,k}} - \mathbf{J}_{\theta_{6,k}}\right) & \mathbf{J}_{r_{5,k}} \end{bmatrix},$$

$$\mathbf{J}'_{6,k} = \begin{bmatrix} \mathbf{J}_{\alpha_{6,k}} & \mathbf{J}_{d_{6,k}} & \mathbf{J}_{r_{6,k}} \end{bmatrix},$$

$$\mathbf{J}'_{7,k} = \begin{bmatrix} \mathbf{J}_{\alpha_{7,k}} & \mathbf{J}_{d_{7,k}} & \mathbf{J}_{\theta_{7,k}} & \mathbf{J}_{r_{7,k}} \end{bmatrix},$$

$$\mathbf{J}'_{E,k} = \begin{bmatrix} \mathbf{J}_{\beta_{E,k}} & \mathbf{J}_{\alpha_{E,k}} & \mathbf{J}_{d_{E,k}} & \mathbf{J}_{r_{E,k}} \end{bmatrix},$$

$$\mathbf{J}'_{8,k} = \begin{bmatrix} -a_{8,k}a_{3,k}\mathbf{J}_{\theta_{3,k}} & -b_{8,k}a_{3,k}\mathbf{J}_{\theta_{3,k}} & -c_{8,k}a_{3,k}\mathbf{J}_{\theta_{3,k}} \\ -d_{8,k}a_{3,k}\mathbf{J}_{\theta_{3,k}} & -e_{8,k}a_{3,k}\mathbf{J}_{\theta_{3,k}} \end{bmatrix},$$

$$\mathbf{J}'_{9,k} = \begin{bmatrix} c_{3,k}\mathbf{J}_{\theta_{3,k}} \end{bmatrix},$$

$$\mathbf{J}'_{10,k} = \begin{bmatrix} d_{3,k}\mathbf{J}_{\theta_{3,k}} \end{bmatrix},$$

$$\mathbf{J}'_{11,k} = \begin{bmatrix} e_{3,k}\mathbf{J}_{\theta_{3,k}} \end{bmatrix}.$$

and :

$$\Delta\boldsymbol{\eta} = [\Delta\alpha_1 \ \Delta d_1 \ \Delta\theta_1 \ \Delta r_1 \ \Delta\alpha_2 \ \Delta d_2 \ \Delta r_2 \ \Delta r'_2 \ \Delta\kappa_2 \ \Delta\lambda_2 \ \Delta l_{12} \ \Delta l_{32} \ \Delta\beta_3 \ \Delta\alpha_3 \ \Delta d_3 \ \Delta r_3 \ \Delta\alpha_4 \ \Delta d_4 \ \Delta\theta_4 \ \Delta r_4 \ \Delta\alpha_5 \ \Delta d_5 \ \Delta\theta_5 \ \Delta r_5 \ \Delta\alpha_6 \ \Delta d_6 \ \Delta r_6 \ \Delta\alpha_7 \ \Delta d_7 \ \Delta\theta_7 \ \Delta r_7 \ \Delta\beta_E \ \Delta\alpha_E \ \Delta d_E \ \Delta r_E \ \Delta r'_8 \ \Delta\kappa_8 \ \Delta\lambda_8 \ \Delta l_{18} \ \Delta l_{38} \ \Delta d_9 \ \Delta d_{10} \ \Delta d_{11}]^T.$$

As one can see, for each robot joint configuration k, the calculation of the (6x43) matrix $\mathbf{J}'_{G,k}$ allows to calculate the effects of the 43 geometrical errors $\Delta\boldsymbol{\eta}$ onto the positioning error $\Delta\mathbf{X}_{E,k}$. Among them, 29 are related to the description of the robot structure [14, 15], 5 are necessary to model the errors in each ball screw and only 4 (one angular and one dimensional parameters are assumed to be known) parameters have been used to model the positioning errors of the spindle onto the robot fringe.

This resulting error model will be used for both sensitivity, identifiability study and linear identification of the geometrical errors during calibration process [8, 16]. The error model could have been more accurate by integrating the gear ratio of the actuators.

IV. Elastic Modelling

The purpose of this part is to evaluate the elastic deformations of the robot structure when a wrench is applied onto the end-effector E during machining [2-5, 10]. In order to derive the stiffness model of the KUKA, all links of the closed-loop kinematic chain are considered as beams and nodes. The method that we recently proposed in [17] is involved to derive in an analytical way, the stiffness matrix of the structure. The assumptions that we made to derive the stiffness model the KUKA structure are the following ones:

- The beam theory is applicable to all links.
- The wrist is stiff enough to be neglected in the stiffness modelling (rigid body).
- The structure is modelled only in the plane $(O_1\mathbf{x}_1\mathbf{z}_1)$ since the model can be easily extended to the space by identifying the stiffness matrix of joint 1 separately by acting on joint 1 and keeping the other joints blocked (not presented in the paper). For the elastic modelling, all nodes of the robot have been numbered (see Fig. 9). This numbering is deduced from the geometrical modelling previously achieved with the beam indexes $b = 1,..,6$.

A. Nodal displacement and nodal wrench

Expressed in the reference frame R_b of the beam B_b, the wrench acting on the node j is defined by $\mathbf{F}_j = [F_{Xj}\ F_{Yj}\ F_{Zj}\ M_{Xj}\ M_{Yj}\ M_{Zj}]^T$. The corresponding displacement due to $\mathbf{F}_j$ is $\Delta\mathbf{X}_j = [d\mathbf{P}_j\ \boldsymbol{\delta}_j]^T$, where $d\mathbf{P}_j = [u_j\ v_j\ w_j]^T$ stands for the vector of the elastic linear displacements and $\boldsymbol{\delta}_j = [\theta_{Xj}\ \theta_{Yj}\ \theta_{Zj}]^T$ stands for the vector of elastic rotation displacements (Fig. 8).

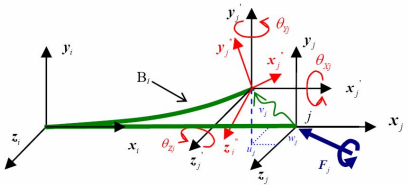

Fig. 8 Nodal wrench and nodal displacement.

B. Stiffness matrix of the links

Based on the numbers used in Fig. 9, the stiffness matrix links the nodal i and j wrenches to the nodal displacements. The stiffness matrix of an element depends on its geometrical and mechanical parameters. These parameters are recalled in Table III.

TABLE III
GEOMETRICAL AND MECHANICAL PARAMETERS.

Geometrical Parameters	Length & Cross-sectional area	L & S
Mechanical Parameters	Young's & Coulomb's modulus	E & G
	Quadratic & Polar moments	I_y, I_z & J

For a beam B_b defined by two nodes i and j, the stiffness matrix is a well-known 12 dimensional square matrix ${}^{R_b}\mathbf{K}^b$. Defined in its local coordinate system R_b, it can be expressed by using four sub-matrices as follows:

$$ {}^{R_b}\mathbf{K}^b = \left[\begin{array}{c|c} {}^{R_b}\mathbf{K}^b_{ii} & {}^{R_b}\mathbf{K}^b_{ij} \\ \hline {}^{R_b}\mathbf{K}^b_{ji} & {}^{R_b}\mathbf{K}^b_{jj} \end{array}\right]. \quad (16)$$

${}^{R_b}\mathbf{K}^b$ components can be expressed in the global coordinate system R_0 by the relation: ${}^{R_0}\mathbf{K}^b = \mathbf{P}_b^{-1}\ {}^{R_b}\mathbf{K}^b\ \mathbf{P}_b$, with:

$$ \mathbf{P}_b = \begin{bmatrix} \mathbf{G}_b & \mathbf{0}_3 & \mathbf{0}_3 & \mathbf{0}_3 \\ \mathbf{0}_3 & \mathbf{G}_b & \mathbf{0}_3 & \mathbf{0}_3 \\ \mathbf{0}_3 & \mathbf{0}_3 & \mathbf{G}_b & \mathbf{0}_3 \\ \mathbf{0}_3 & \mathbf{0}_3 & \mathbf{0}_3 & \mathbf{G}_b \end{bmatrix}. \quad (17)$$

Matrix $\mathbf{G}_b$ (3x3) stands for the rotation matrix from the local coordinate system R_b to the global coordinate system R_0. $\mathbf{G}_b$ is calculated during the geometrical modelling. ${}^{R_0}\mathbf{K}^b$ is the stiffness matrix formulated in the global frame R_0:

$$ {}^{R_0}\mathbf{K}^b = \left[\begin{array}{c|c} {}^{R_0}\mathbf{K}^b_{ii} & {}^{R_0}\mathbf{K}^b_{ij} \\ \hline {}^{R_0}\mathbf{K}^b_{ji} & {}^{R_0}\mathbf{K}^b_{jj} \end{array}\right]. \quad (18)$$

C. Stiffness matrix of deformable joints

To fully describe the elastic behaviour of the closed-loop kinematic chain, the compliance of the joints has to be integrated in the model. In a first approach, we assume that the used compliance matrix expressed in its local frame $R^{u,v}$ between nodes u and v is given by:

$$ {}^{R^{u,v}}\mathbf{K}^{u,v} = \left[\begin{array}{c|c} {}^{R^{u,v}}\mathbf{K}^{u,v} & -{}^{R^{u,v}}\mathbf{K}^{u,v} \\ \hline -{}^{R^{u,v}}\mathbf{K}^{u,v} & {}^{R^{u,v}}\mathbf{K}^{u,v} \end{array}\right], \quad (19)$$

with: ${}^{R^{u,v}}\mathbf{K}^{u,v} = \mathrm{diag}\left[K_r^{u,v}\ \ K_r^{u,v}\ \ K_a^{u,v}\ \ K_{rr}^{u,v}\ \ K_{rr}^{u,v}\ \ K_{ar}^{u,v}\right]$.

In this expression, $K_r^{u,v}$ and $K_a^{u,v}$ stand respectively for the axial and the radial stiffness of the revolute joint between nodes u and v. $K_{ar}^{u,v}$ and $K_{rr}^{u,v}$ are the axial rotational and the radial translational stiffness.

In this way, for the passive joints 3, 9 and 10 on Fig. 2, the axial rotational stiffness is close to zero. However, for numerical problems, $K_{ar}^{u,v}$ cannot be null. So it has been chosen to set this parameter to 10^{-7} N.rad^{-1}. For the active joints 2 and 8, the parameter stands for the axial stiffness of the actuator. By identification through measurements made directly on the robot [17], the stiffness of the joints has been identified and the $K_{ar}^{u,v}$ parameters for the active joints have been identified to 2.10^9 N.rad^{-1} using the Matlab's *lsqnonlin* function. The mechanical parameters of the beam keep their nominal values calculated using the nominal dimensions of the links.

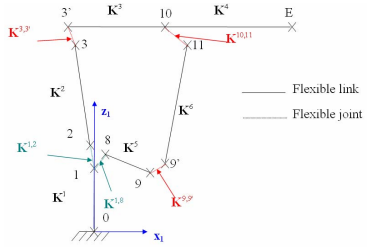

Fig. 9. Elastic modelling with deformable joints.

The well-known stiffness assembly technique involved in matrix structural analysis is then used to derive the global stiffness matrix ${}^0\mathbf{K}_G$ of the robot structure [18]. For that purpose, all the stiffness matrices of the beams of Fig. 9 are expressed within the reference frame R_0 and they are then mapped into a global matrix as follows:

$$ {}^0\mathbf{K}_G = \left[\begin{array}{c|c} {}^{R_0}\mathbf{K}_1 & {}^{R_0}\mathbf{K}_3^T \\ \hline {}^{R_0}\mathbf{K}_3 & {}^{R_0}\mathbf{K}_2 \end{array}\right]_{66\times 66}, \quad (20)$$

where:

$$ {}^{R_0}\mathbf{K}_1 = \begin{array}{c} \begin{array}{ccccccc} 0 & 1 & 2 & 3 & 3' & 10 & E \end{array} \\ \begin{bmatrix} \mathbf{K}^1_{00} & \mathbf{K}^1_{01} & \mathbf{0}_6 & \mathbf{0}_6 & \mathbf{0}_6 & \mathbf{0}_6 & \mathbf{0}_6 \\ \mathbf{K}^1_{10} & \mathbf{K}^1_{11}+\mathbf{K}^{1,2}+\mathbf{K}^{1,8} & -\mathbf{K}^{1,2} & \mathbf{0}_6 & \mathbf{0}_6 & \mathbf{0}_6 & \mathbf{0}_6 \\ \mathbf{0}_6 & -\mathbf{K}^{1,2} & \mathbf{K}^2_{22}+\mathbf{K}^{1,2} & \mathbf{K}^2_{23} & \mathbf{0}_6 & \mathbf{0}_6 & \mathbf{0}_6 \\ \mathbf{0}_6 & \mathbf{0}_6 & \mathbf{K}^2_{32} & \mathbf{K}^2_{33}+\mathbf{K}^{3,3'} & -\mathbf{K}^{3,3'} & \mathbf{0}_6 & \mathbf{0}_6 \\ \mathbf{0}_6 & \mathbf{0}_6 & \mathbf{0}_6 & -\mathbf{K}^{3,3'} & \mathbf{K}^3_{3'3'}+\mathbf{K}^{3,3'} & \mathbf{K}^3_{3'10} & \mathbf{0}_6 \\ \mathbf{0}_6 & \mathbf{0}_6 & \mathbf{0}_6 & \mathbf{0}_6 & \mathbf{K}^3_{103'} & \mathbf{K}^3_{1010}+\mathbf{K}^4_{1010}+\mathbf{K}^{10,11} & \mathbf{K}^4_{E11} \\ \mathbf{0}_6 & \mathbf{0}_6 & \mathbf{0}_6 & \mathbf{0}_6 & \mathbf{0}_6 & \mathbf{K}^4_{E10} & \mathbf{K}^4_{EE} \end{bmatrix} \end{array}, $$

$$ {}^{R_0}\mathbf{K}_2 = \begin{array}{c} \begin{array}{cccc} 8 & 9 & 9' & 11 \end{array} \\ \begin{bmatrix} \mathbf{K}^5_{88}+\mathbf{K}^{1,8} & \mathbf{K}^5_{89} & \mathbf{0}_6 & \mathbf{0}_6 \\ \mathbf{K}^5_{98} & \mathbf{K}^5_{99}+\mathbf{K}^{9,9'} & -\mathbf{K}^{9,9'} & \mathbf{0}_6 \\ \mathbf{0}_6 & -\mathbf{K}^{9,9'} & \mathbf{K}^6_{9'9'}+\mathbf{K}^{9,9'} & \mathbf{K}^6_{9'11} \\ \mathbf{0}_6 & \mathbf{0}_6 & \mathbf{K}^6_{119'} & \mathbf{K}^6_{1111}+\mathbf{K}^{10,11} \end{bmatrix} \end{array}, $$

$$ {}^{R_0}\mathbf{K}_3 = \begin{bmatrix} \mathbf{0}_6 & -\mathbf{K}^{1,8} & \mathbf{0}_6 & \mathbf{0}_6 & \mathbf{0}_6 & \mathbf{0}_6 & \mathbf{0}_6 \\ \mathbf{0}_6 & \mathbf{0}_6 & \mathbf{0}_6 & \mathbf{0}_6 & \mathbf{0}_6 & \mathbf{0}_6 & \mathbf{0}_6 \\ \mathbf{0}_6 & \mathbf{0}_6 & \mathbf{0}_6 & \mathbf{0}_6 & \mathbf{0}_6 & \mathbf{0}_6 & \mathbf{0}_6 \\ \mathbf{0}_6 & \mathbf{0}_6 & \mathbf{0}_6 & \mathbf{0}_6 & \mathbf{0}_6 & -\mathbf{K}^{10,11} & \mathbf{0}_6 \end{bmatrix}. $$

The vectors ${}^0\mathbf{\Delta X}_G$ and ${}^0\mathbf{F}_G$ that describe the nodal displacements and the nodal wrenches of the structure expressed within R_0 are defined as follows:

$$ {}^0\mathbf{\Delta X}_G = \left[{}^0\mathbf{\Delta X}_0 \quad {}^0\mathbf{\Delta X}_1 \quad \cdots \quad {}^0\mathbf{\Delta X}_9, \quad {}^0\mathbf{\Delta X}_{11} \right]^T, \quad (21) $$

$$ {}^0\mathbf{F}_G = \left[{}^0\mathbf{F}_0 \quad {}^0\mathbf{F}_1 \quad \cdots \quad {}^0\mathbf{F}_9, \quad {}^0\mathbf{F}_{11} \right]^T. \quad (22) $$

D. Boundary conditions

Boundary conditions are introduced to express the fact that the robot is embedded in the ground at the node 0. These conditions are expressed by the system:

$$ \begin{cases} d\mathbf{P}_0 = \mathbf{0}_{3,1} \\ \boldsymbol{\delta}_0 = \mathbf{0}_{3,1} \end{cases}. \quad (23) $$

To integrate these conditions, the size of the stiffness matrix ${}^0\mathbf{K}_G$ has been reduced by deleting the rows and the columns corresponding to the blocked displacements. Its new dimension is (60x60).

As the boundary conditions are perfectly defined, preventing any possibilities of overall displacements of the structure, the stiffness matrix is symmetric positive definite and then invertible (see [17]). Hence the nodal displacements ${}^0\mathbf{\Delta X'}_G$ of the closed loop kinematic chain can be obtained according the relation:

$$ {}^0\mathbf{\Delta X'}_G = {}^0\mathbf{K'}_G^{-1} \, {}^0\mathbf{F'}_G. \quad (24) $$

From that last relation, the positioning error ${}^0\mathbf{\Delta X}_E$ of the end-effector E due to the elastic deformations of the structure can be calculated as a function of ${}^0\mathbf{F'}_G$ and then as a function of the wrench ${}^0\mathbf{F}_E$ applied directly on E during the process (machining).

E. Validation of the stiffness model

In order to verify the validity of the stiffness model, the elastic displacements derived from the proposed model have been compared first with the ones given by a FEA model of the robot achieved on CASTEM® software. As one can see in Table IV, the analytical results do fit well with those obtained through CASTEM®. This can be explained by the fact that this software uses the same method as the one that we applied to derive the elastic model. Contrary to the FEA modelling, the analytical model can be used for real time compensation of the elastic deformations

TABLE IV
COMPARISON BETWEEN ANALYTICAL AND FEA MODELS

	θ_2 = 15° θ_8 = -7°		θ_2 = -12° θ_8 = 16°	
	Castem	Analytique	Castem	Analytique
u_E (µm)	12,71	12,71	-32,45	-32,45
v_E (µm)	15,08	15,08	7,91	7,91
w_E (µm)	702,62	702,62	451,62	451,62
θ_{x7} (10^{-6} rad)	-296,94	-296,94	-323,84	-323,84
Θ_{y7} (10^{-6} rad)	-323,12	-323,12	-137,21	-137,21
Θ_{z7} (10^{-6} rad)	14,76	14,76	-32,26	-32,26

The real elastic displacements have then been measured on the KUKA by using the same measurement system that the one we used in [17] (Fig. 10). This system allows measuring the three translational displacements of the E due to the elastic deformations of the structure under loads applied on E. Three loads of 30, 60 and 100 kg have been used. The norms of the measured displacements within the plane $(O_1\mathbf{x}_1\mathbf{z}_1)$ are summarized by Fig. 11. They show the the elastic significant deformations of the structure. The norm of these measured displacements has then been compared to those calculated with the proposed model. As shown in Fig. 12 (a), the calculated measurements fit well with the realistic elastic behaviour of the robot.

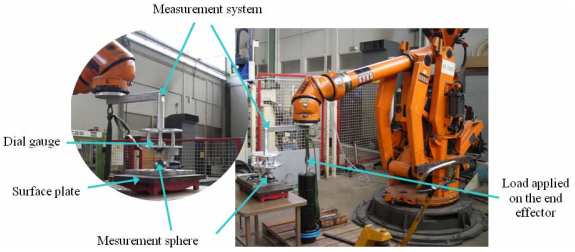

Fig. 10. Methodology of measurement.

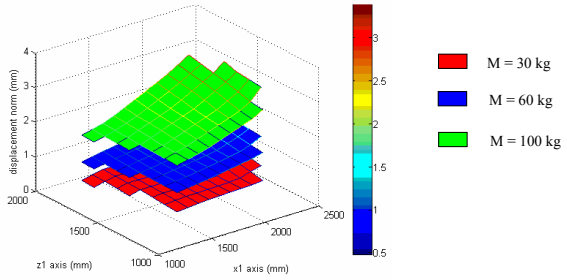

Fig. 11. Measured elastic displacements.

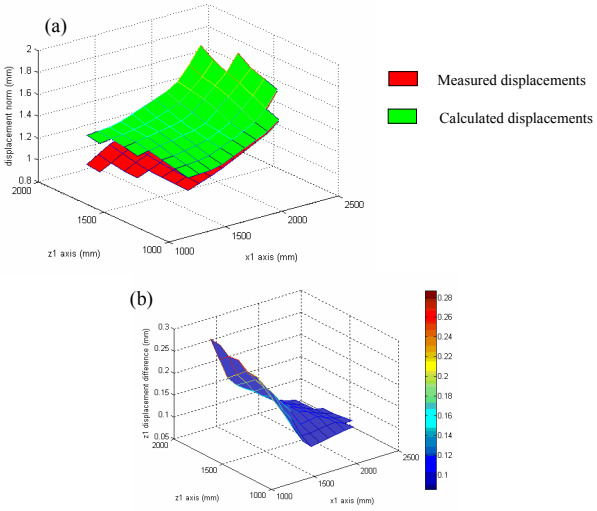

Fig. 12. Comparison between analytical model with flexible joints and measured displacements for 60 kg load, (a) : norm of the displacements, (b) : displacement difference along $\mathbf{z}_1$ axis

F. Discussion

Another elastic model has been established by considering all the joints of the closed loop as perfectly rigid. The comparison between that last model and the previous one has shown that the main source of flexibility is related to the compliance in the joints. It has been shown by simulations that the links deformations represent only 20% of the overall elastic displacement of E. This can be easily understood if one considers the design of the robot parts which gives them a high level of stiffness.

Moreover, we can see on Fig. 12 (a) and (b) that the norm of the displacement is well estimated when the wrist is far from $\mathbf{z}_1$ axis (along $\mathbf{x}_1$ axis). On the contrary, when the end-effector E is moved by the structure close to $\mathbf{z}_1$ axis, the model is too stiff and do not fit anymore with the reality. To our thinking, this is due to the fact that the stiffness of the two ball screws has been represented by a equivalent stiffness located only at the center of the joints 2 and 8. This does not fit with the reality and a better model should have described each ball screw by using extra beams connected to the robot links 2 and 8 on one hand and to the first link through prismatic and revolute joints on the other hand (Fig. 13.).

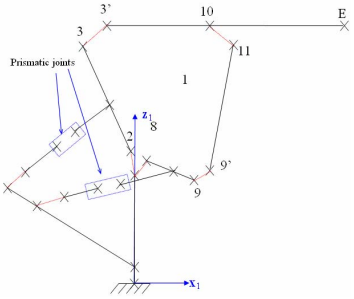

Fig. 13. Elastic modelling integrating the ball screws.

V. Conclusion and Perspectives

In this paper, we have presented the elasto-geometrical modelling of an industrial robot including a closed-loop kinematic chain actuated by two slider crank type mechanisms. The main originality of that work is that both the geometrical and elastic error models have been derived in a systematic analytical way. These models will be now involved to study in a first time, the sensitivity of the robot positioning accuracy to the geometrical and elastic parameter errors of its structure. Then, in a second time, its elasto-geometrical calibration will be achieved in order to enhance its global positioning accuracy for machining.

To our thinking, the same approach could be used to derive the elasto-geometrical models of other serial structures used for quasi static tasks that require a high level of accuracy. Moreover, due to the fact that the formulation of the elastic model is analytical, it could be implemented in the robot controller for a real-time compensation of the tool elastic positioning errors.

References

[1] C. Bates, "Move over machine tools here come robots," in *American Machinist*, 2006.

[2] K. Schroer, S. L. Albright, and A. Lisounkin, "Modeling closed-loop mechanisms in robots for purposes of calibration," *Robotics and Automation, IEEE Transactions on*, vol. 13, pp. 218-229, 1997.

[3] T. Tsumugiwa, R. Yokogawa, and K. Hara, "Measurement Method for Compliance of Vertical-Multi-Articulated Robot-Application to 7-DOF Robot PA-lO," presented at The IEEE International Conference on Robotics and Automation, Taipei, Taiwan, 2003.

[4] G. Alici and B. Shirinzadeh, "Enhanced Stiffness Modeling, Identification and Characterization for Robot Manipulators," *IEEE Transactions on Robotics and Automation*, vol. 21, pp. 554-564, 2005.

[5] H. R. Choi, W. K. Chung, and Y. Youm, "Stiffness analysis and control of redundant manipulators," 1994.

[6] H. Nakamura, T. Itaya, K. Yamamoto, and T. Koyama, "Robot autonomous error calibration method for off line programming system," presented at The IEEE International Conference on Robotics & Automation, Nagoya, Japan, 1996.

[7] W. Khalil and J.-F. Kleinfinger, "A new geometric notation for open and closed loop robots," presented at IEEE Int. Conf. on Robotics and Automation, San Francisco, California, USA, 1986.

[8] W. Khalil and E. Dombre, *Modeling, Identification and Control of Robots*: Hermes Penton Ltd, 2002.

[9] D. J. Bennet and J. M. Hollerbach, "Self-Calibration of Single-loop, Closed Kinematic Chains Formed by Dual and Redundant Manipulators," presented at The 27th IEEE Conference on Decision and Control, Austin, TX, USA, 1988.

[10] M. Rognant and P. Maurine, "Elasto-Geometrical Modelling of a Pantographic Linkage Used as Coordinate Measuring Arm for PKM Applications," presented at 12th IFToMM World Congress, Besançon, France, 2007.

[11] R. Judd and A. Knasinski, "A technique to calibrate industrial robots with experimental verification," *IEEE Transaction on Robotics and Automation*, vol. 6, pp. 20-30, 1990.

[12] L. Everett, "Forward calibration of closed-loop jointed manipulators," *The International Journal of Robotics Research*, vol. 8, pp. 85-91, 1989.

[13] S. Hayati, "Robot arm geometrical link parameter estimation," presented at The 22nd International IEEE Conference on Decision and Control, San Antonio, Texas, USA, 1983.

[14] L. Everett, M. Driels, and B. Mooring, "Kinematic modelling for robot calibration," presented at The IEEE International Conference on Robotics and Automation, 1987.

[15] W. Khalil, M. Gautier, and C. H. Enguehard, "Identifiable parameters and optimum configurations for robot calibration," *Robotica*, vol. 9, pp. 63-70, 1991.

[16] S. Caro, P. Wenger, B. Fouad, and D. Chablat, "Sensitivity analysis of the Orthoglide: a three-dof translational parallel kinematic machine," *Transaction of the ASME*, vol. 128, pp. 392-402, 2006.

[17] D. Deblaise, X. Hernot, and P. Maurine, "A Systematic Analytical Method for PKM Stiffness Matrix Calculation," presented at IEEE International Conference on Robotics and Automation, Orlando, Florida, USA, 2006.

[18] H. C. Martin, *Introduction to matrix methods of structural analysis*: McGraw-Hill Book Company, 1966.